Ground and space signatures of VLF noise suppression by whistlers

D. R. Shklyar,[1,2] **J. Manninen,**[3] **E. E. Titova,**[4,1] **O. Santolík,**[5,6] **I. Kolmašová,**[5,6] **and T. Turunen**[3]

[1]Space Research Institute, Russian Academy of Sciences, Moscow, Russia.
[2]National Research University Higher School of Economics, Moscow, Russia.
[3]Sodankylä Geophysical Observatory, Sodankylä, Finland.
[4]Polar Geophysical Institute, Apatity, Russia.
[5]Department of Space Physics, Institute of Atmospheric Physics, Czech Academy of Sciences, Prague, Czechia.
[6]Faculty of Mathematics and Physics, Charles University, Prague, Czechia.

Key Points:

- Masked VLF wave phenomena are revealed by "cleaning" from sferics spectrograms registered at Kannuslehto ground station.
- VLF noise suppression by strong whistlers is due to whistler related modification of electron distribution in the noise generation region.
- This modification is caused by phase space diffusion of energetic electrons in the field of multihop whistler.

Corresponding author: J. Manninen, Jyrki.Manninen@sgo.fi

Abstract

VLF spectrograms registered at Kannuslehto ground station, after cleaning them from strong sferics, reveal VLF noise suppression by whistlers and whistler echo trains, which consists in significant reduction in the noise spectral power after a strong whistler event. We have found similar effect in the VLF data from Van Allen Probe B taken in the equatorial region on L-shell ~ 3. Detailed analysis of the data shows that the whistler echo train as well as the VLF noise have small wave normal angles. Based on this observation, we limit our analysis to parallel (ducted) whistler wave propagation. The persistence of whistler echo train as well as the VLF noise suggests that in the events under discussion, plasma is unstable in the frequency range corresponding to the observed VLF noise band. In an attempt to explain the effect of VLF noise suppression, we follow up the long-standing idea that relates this effect to the reduction of free energy in the unstable plasma distribution by whistler echo train. To develop this idea into qualitative model, we have studied the motion of energetic electrons, responsible for the noise generation, in the field of ducted whistler echo train. We show that energetic electrons that make the main contribution to the growth rate of VLF noise, during their bounce oscillations in the magnetosphere are subject to multiple resonant impacts from the whistler echo train. These lead to energetic electron diffusion in the phase space, and the corresponding reduction in free energy of the unstable distribution.

1 Introduction

In this paper we discuss the wave phenomenon in VLF frequency band which consists in transient reduction in the amplitude of VLF noise observed, first on the ground, after receiving a strong whistler. An example of this phenomenon is shown in Figure 1, which displays the spectrogram in the frequency band up to 8 kHz registered at Kannuslehto ground station in Finland on 25 December 2011. The upper panel shows the wave magnetic field power spectral density over a 4 minute interval. A significant decrease in spectral amplitude of VLF noise after receiving a strong whistler is clearly visible. We will turn our attention to other panels of Figure 1 later on. Other examples of VLF noise suppression by strong whistler echo trains, registered at Kannuslehto ground station, may be found in the supplementary material to the paper.

Suppression effect under discussion was known for a long time. Based on observations on Siple Station, *Helliwell et al.* [1980] reported one-to-one correlation between hiss and optical emission ($\lambda 4278$) intensity reductions immediately following each discrete VLF event.

Since optical emission was assumed to result from particle precipitation, the authors suggested that both the hiss and optical emission reductions were caused by pitch angle scattering of energetic electrons by whistlers.

A comprehensive study of whistler induced suppression of VLF noise has been performed by *Gail and Carpenter* [1984]. The authors have established several important features of the suppression effect, in particular, they demonstrated that the effect usually occurs when the driving whistler exhibits echoes confined to the frequency band occupied by the suppressed noise. They have also shown that the recovery of the noise band to the pre-event level takes several seconds, and this time correlates with the damping rate of the echo train. The effect of suppression of the VLF noise band produced by the whistler that triggered it has been reported by *Platino et al.* [2005] basing on observations by the Cluster spacecraft.

The explanation of the noise suppression suggested by *Helliwell et al.* [1980] and accepted by *Gail and Carpenter* [1984] consists in pitch angle scattering of energetic electrons by the whistler signal that leads to disruption of wave amplification in the magnetospheric interaction region. Those electrons which are scattered into the loss cone are observed as precipitation, providing the correlation between $\lambda 4278$ optical emission and VLF noise suppression. We should mention that, although the pitch angle scattering may lead to reduction in the particle pitch angle anisotropy and, thus, decrease the amplification efficiency, the electrons close to the loss cone do not contribute significantly to the noise amplification due to small amplitude of interaction between these particles and parallel propagating whistler waves.

2 Experimental features of suppression phenomenon

2.1 Ground based observations

Let us return to Figure 1 which presents the observations of VLF noise suppression by whistlers performed at Kannuslehto ground station (KAN) in Finland (67.74N, 26.27E; $L = 5.5$) on 25 December 2011. As was mention above, the upper panel displays the power spectral density of the wave magnetic field and illustrates the phenomenon under discussion. This spectrogram was preliminary cleaned from sferics using the method described in *Manninen et al.* [2016]. Pay attention that a pronounced decrease in the noise intensity is observed after the second dispersed trace of the whistler echo train. Only the frequency band up to 8 kHz is displayed, although VLF emissions were recorded in the frequency range from 0.2 to 39 kHz. Magnetic field measurements were performed using two mutually orthogonal magnetic

loop antennas oriented in the geographical north-south and east-west directions. This allows us to determine the polarization of waves which is characterized by the parameter p:

$$p = 10 \cdot \log_{10}\left(\frac{|H_{\mathrm{R}}|^2}{|H_{\mathrm{L}}|^2}\right) , \tag{1}$$

where $H_{\mathrm{R,L}} = (H_{\mathrm{N}} \pm i H_{\mathrm{E}})/\sqrt{2}$ are the right- and left-hand polarized horizontal magnetic field components, respectively, and $H_{\mathrm{N,E}}$ are the northward and eastward projections of the wave magnetic field. This parameter, displayed in the middle panel of Figure 1, shows that both whistlers and VLF noise have left-hand polarization, which indicates that the signals come to the Kannuslehto station over the Earth-ionosphere waveguide [*Ostapenko et al.*, 2010]. The lower panel of Figure 1 displays the angle (with an ambiguity of 180^o) between the minor axis of the wave polarization ellipse and the north-south direction, which determines (with the same ambiguity) the direction of wave arrival at the station. Close values of the displayed quantity for both whistlers and noise suggest that they have close exit regions from the ionosphere. As for time characteristics of the noise suppression phenomenon, it becomes the most pronounced about $15 - 30$ seconds after strong whistler event and lasts several tens of seconds.

2.2 Space observations onboard Van Allen Probes (RBSP)

We have not found suppression events in Cluster or RBSP data simultaneous with any one observed at Kannuslehto ground station. And an independent suppression event that we have found in RBSP-B data, and which is discussed below, is quite weak.

Intense whistlers and echo trains were registered onboard RBSP-B on 22 December 2014. VLF spectrogram up to 11 kHz obtained from electric (a) and magnetic (b) field measurements of the EMFISIS instrument [*Kletzing et al.*, 2013] during the time period 19:23:29 - 19:24:23 UT when the instrument operated in the burst mode is shown in Figure 2. During this time RBSP-B was in the morning sector in the southern hemisphere and had the following coordinates: MLT $\sim$ 5 h, MLAT $\sim -18^o$, and $L \sim 3$. Both electric and magnetic receivers registered whistlers, sometimes with their echoes, and VLF noise below 6 kHz. The most intense whistlers were registered at about 19:24 UT, first a fractional-hop whistler at 19:23:57 UT, which came from the southern hemisphere, and then three echo signals, after which a decrease in the VLF noise intensity below 6 kHz can be observed. Minimum intensity of the VLF noise was observed ~ 20 s after the first reflected whistler.

Suppression of the noise intensity by whistler can be clearly seen from Figure 3b which shows electric field spectral density in three narrow frequency channels 3988, 5020, and 5623

Hz in the time interval 19:20 - 19:28 UT. Three distinct spikes of spectral amplitude, which we associate with multihop whistlers (marked by "w" in the figure), followed by decrease in the noise amplitude are clearly seen. Minimum values of the noise intensity marked by arrows are observed $\sim 15 - 30\,\mathrm{s}$ after whistlers.

Figure 3a shows cold plasma density [*Kurth et al.*, 2015] along the satellite trajectory, which smoothly increases between 19:21 and 19:24 UT, then remains almost constant and then slightly decreases after 19:27:30 UT. The amplitudes of whistlers and VLF noise also increase till 19:24 UT, whereupon intense whistlers are not observed, while the amplitude of noise slowly decreases. Simultaneous increase of the cold plasma density and VLF wave amplitudes (both of whistlers and VLF noise) may be related to ducting of whistler waves by density gradient of the cold plasma [*Inan and Bell*, 1977; *Semenova and Trakhtengerts*, 1980].

Ducted propagation of whistlers and VLF noise is confirmed by multicomponent analysis of VLF waves. Figure 4 shows (a) the sum of power spectral densities of three magnetic field components, (b) planarity of the wave magnetic field [*Santolík et al.*, 2002], (c) wave normal angle [*Santolík et al.*, 2003], and (d) a spectral estimate of a polar angle of Poynting vector with respect to the ambient magnetic field [*Santolík et al.*, 2010]. One can see that fractional-hop whistler propagates towards the northern hemisphere, while multihop whistlers propagate towards the southern hemisphere. VLF noise also propagates towards the southern hemisphere. An important result that follows from the multicomponent analysis consists in that both whistlers and VLF noise have small wave normal angles. This suggests that the observed multihop whistlers propagate in ducted mode, and that VLF noise is most probably generated at the equator.

To check the assumption that resonant interaction of energetic electrons with multihop whistlers changes their distribution in such a way that the free energy of the distribution is decreased, leading to the corresponding decrease in the growth rate, we have calculated the growth rates for parallel propagating whistler waves using the data from MagEIS instrument on RBSP-B [*Blake et al.*, 2013]. This growth rate is determined by the expression given in *Sagdeev and Shafranov* [1961]. Assuming that electron distribution function determining the growth rate is the function of particle kinetic energy $w = mv^2/2$ and magnetic momentum $\mu = mv_\perp^2/2\omega_c$ ($m,\ v,\ v_\perp$ are electron mass, total and transverse velocities, respectively, and ω_c is electron cyclotron frequency) this expression takes the form:

$$\gamma_{\text{L}} = \omega \frac{8\pi^3 e^2 \omega_{\text{c}}(\omega_{\text{c}} - \omega)}{m^2 k^3 c^2} \int_0^\infty d\mu f_0'(\mu)\mu \,. \tag{2}$$

Here ω is the wave angular frequency, k is the magnitude of the wave normal vector, e is the magnitude of electron charge, c is the speed of light, and

$$f_0'(\mu) = \left(\frac{\partial f_0}{\partial \mu} + \omega \frac{\partial f_0}{\partial w} \right)_{w = m v_{\mathrm{R}}^2/2 + \mu \omega_{\mathrm{c}}} , \tag{3}$$

where

$$v_{\mathrm{R}} = \frac{\omega - \omega_c}{k} \tag{4}$$

is the resonance velocity at the first cyclotron resonance, the only one that exists at parallel propagation. As it is indicated above, after taking the derivatives in (3), particle parallel velocity is equated to v_{R}, so that the combined derivative (3) becomes a function of the magnetic momentum.

Electron distribution function that enters the above relations is determined from the measured electron differential flux by the relation [*Cornilleau-Wehrlin et al.*, 1985]:

$$f(w, \mu) \simeq 1.67 \cdot 10^{-37} \frac{J}{W} . \tag{5}$$

Relation (5) determines the electron distribution function in CGS system of units, used in the paper, through the measured differential electron flux J expressed in practical units, i.e.,

$$(\mathrm{cm}^{-2} \cdot \mathrm{s}^{-1} \cdot \mathrm{sr}^{-1} \cdot \mathrm{keV}^{-1})$$

and the particle energy in keV denoted by W. We should underline that, no matter in which variables the distribution function is expressed, it is always equal to particle density in the phase space $(\mathbf{r}, \mathbf{v})$.

Normalized growth rates calculated from RBSP-B data for various moments before and after strong whistler events are shown in Figures 5-6. We see that the decrease of growth rate after one whistler event is quite small, although the decrease of growth rate after the series of three multihop whistlers is significant. Qualitative explanation of this result follows from the consideration in the next section.

While the decrease in the growth rate related to strong whistler events is clearly seen in Figures 5-6, the unstable frequency band does not correspond to that of equatorial VLF noise. The reason for this is that those growth rates are local, calculated at the latitude $\sim -18.6^o$, but not at the equator where the VLF noise is supposed to be generated. At the latitude $\sim -18.6^o$ the loss-cone is wider than at the equator, while the cyclotron frequency and, thus, the resonance velocity are larger. Due to these, outside the equator we should expect smaller values

of the growth rate, but wider unstable frequency range. This is confirmed by direct calculation of the growth rate at the equator, at the same L-shell where the suppression phenomenon has been observed, but at other time. This growth rate is shown in Figure 7. We see that at the equator, the growth rate is one order of magnitude larger than outside the equator, and the frequency of the growth rate maximum corresponds much better to the observed frequency band of VLF noise.

3 Qualitative model of the VLF noise suppression by whistlers

3.1 Main assumptions of the model

A general idea, which has been put forward by *Helliwell et al.* [1980] and *Gail and Carpenter* [1984] for explanation of the wave phenomenon under discussion, consists in the modification of the electron distribution function by whistler in the way that reduces plasma instability causing the hiss generation. In the present study we follow up this idea and develop it into a qualitative model. A few assumptions suggested by observations that we use are the following.

1. VLF noise is generated in the equatorial region of the magnetosphere by unstable plasma distribution, and is characterized by a quasi-parallel direction of the wave normal vectors.
2. Whistler echo train causing the noise suppression propagates in ducted mode and can be describe in the approximation of parallel propagation.
3. At the pre-event stage, the plasma is in a marginally unstable state, the upper frequency of the observed noise band corresponding to the boundary between unstable and stable frequency bands.
4. In the magnetospheric region, where the strong whistler interactions with resonant electrons responsible for the noise generation takes place, the electromagnetic field of the whistler echo train can be represented as a sum of three wave packets with varying frequencies and wave numbers; the frequency range of the causative whistler echo train overlaps the frequency band occupied by the suppressed noise.
5. While the strong whistler changes the energetic particle distribution, the generation of VLF hiss may be described in linear approximation, i.e., neglecting the back influence of the noise upon resonant particle distribution.

3.2 Energetic electron motion in the field of whistler echo train

Since VLF noise suppression is usually observed after the second dispersed whistler trace, we will assume the wave field to consist of three wave packets: a fractional-hop whistler originating from a lightning stroke in the southern hemisphere (for the sake of definiteness), and two reflected whistlers, one from the northern and one from the southern hemisphere. Based on experimental observations, we will assume parallel propagation of all waves, which essentially simplifies the problem. In the case of parallel propagation, the wave field has only x- and y-components, transverse to the direction of wave propagation. Thus, we will write the wave electric field in the form:

$$E_x(z,t) = -\sum_i E_{0i}(z,t)\cos\Psi_i(z,t) \quad E_y = \sum_i E_{0i}(z,t)\sin\Psi_i(z,t)\ ; \quad (i=1,2,3)\ , \tag{6}$$

where z is the coordinate along the ambient magnetic field, $E_{0i}(z,t),\ \Psi_i(z,t)$ are amplitudes and phases of the i-th wave packet. In the following numerical calculations, we will not consider space-time variation of the wave amplitudes, but will put them equal to $8\,\mathrm{mV/m}$ wherever the wave packets exist. At the same time, we will use exact expressions for wave packet phases as they follow from the equations of geometrical optics.

The wave frequency and the wave normal vector in each wave packet are determined in the usual way:

$$\omega_i(z,t) = -\frac{\partial\Psi_i(z,t)}{\partial t} \quad k_{zi}(z,t) \equiv k_i(z,t) = \frac{\partial\Psi_i(z,t)}{\partial z}\ . \tag{7}$$

In each wave packet, the wave frequency $\omega_i(z,t)$ and the wave normal vector $k_i(z,t)$ depend on both coordinate z and time t, but for each z and t they are related by the dispersion relation for parallel propagating whistler mode waves, namely:

$$\frac{k^2(z,t)\,c^2}{\omega^2(z,t)} = 1 + \frac{\omega_p^2(z)}{\omega(z,t)[\omega_c(z) - \omega(z,t)]}\ , \tag{8}$$

where $\omega(z,t)$ and $k(z,t)$ are the frequency and the wave number defined above which depend on (z,t), $\omega_p(z)$ is electron plasma frequency that depends on z, $\omega_c(z)$ is, as before, the electron cyclotron frequency which also depends on z. The wave frequency in each wave packet calculated from the equations of geometrical optics under assumption of parallel propagation is shown in Figure 8. For given frequency $\omega(z,t)$ and coordinate z, the wave number $k(z,t)$, up to its sign, is determined by (8). For the first and the third wave packets $k(z,t) > 0$, while for the second wave packet $k(z,t) < 0$.

In non-relativistic approximation, and for parallel propagating whistler-mode wave, the resonance between the wave and electron arises under condition $v_\parallel = (\omega - \omega_c)/k$. Corre-

spondingly, electron resonance parallel energy in keV, with the account of (8), is given by

$$w_{\parallel res}(z,t) \equiv \frac{m[\omega(z,t)-\omega_c(z)]^2}{2k^2(z,t)}\frac{1}{\mathrm{keV}} \simeq 256\cdot\frac{[\omega_c(z)-\omega(z,t)]^3}{\omega(z,t)\omega_p^2(z)}\ , \tag{9}$$

where keV $= 1.6\cdot 10^{-9}$. The quantity $w_{\parallel res}(z,t)$ in space-time domains where the multi-hop whistler exists is shown in Figure 9.

The wave electric field in the form (6) corresponds to right-hand polarization with respect to the ambient magnetic field independently of the sign of wave number k, i.e., of the direction of the wave propagation. In our case, k_1 and k_3 are positive, while k_2 is negative. The wave magnetic field can be found from the wave electric field (6) using the Faraday induction law.

In the absence of the wave field, particle kinetic energy w and magnetic momentum μ are conserved, and the particle motion can be described by the equations that follow from the unperturbed Hamiltonian

$$H_0 = \frac{p_\parallel^2}{2} + \mu\omega_c(z)\ , \tag{10}$$

where canonically conjugated variables are $(p_\parallel, z)$ and (μ,φ), where φ is the particle gyrophase. Transverse components of electron velocity are expressed in canonical variables as follows:

$$v_x = \sqrt{\frac{2\mu\omega_c(z)}{m}}\cos\varphi\ ;\quad v_y = \sqrt{\frac{2\mu\omega_c(z)}{m}}\sin\varphi\ . \tag{11}$$

We now write the variation of electron kinetic energy due to interaction with the whistler echo train:

$$\frac{dw}{dt} \equiv -e\mathbf{E}\mathbf{v} = e\sqrt{\frac{2\mu\omega_c(z)}{m}}\sum_i E_{0i}\cos[\Psi_i(z,t)+\varphi]\ , \tag{12}$$

where $-e$ is electron charge. As has been shown by *Shklyar and Matsumoto* [2009], for resonant particles, the rate of energy variation coincides with partial derivative of the interaction Hamiltonian with respect to time. Taking this into account, and making use of (10) we come to the expression for the total Hamiltonian of the problem in the form

$$H = \frac{p_\parallel^2}{2} + \mu\omega_c(z) - e\sqrt{\frac{2\mu\omega_c(z)}{m}}\sum_i \frac{E_{0i}}{\omega_i(z,t)}\sin[\Psi_i(z,t)+\varphi]\ . \tag{13}$$

The equations of motion which follow from the Hamiltonian (13) have the form:

$$\begin{aligned}
\frac{dz}{dt} &= \frac{p_\parallel}{m}\ ;\quad \frac{dp_\parallel}{dt} = -\mu\frac{d\omega_c}{dz} + e\sqrt{\frac{2\mu\omega_c(z)}{m}}\sum_i \frac{E_{0i}k_i(z,t)}{\omega_i(z,t)}\cos[\Psi_i(z,t)+\varphi]\ ; \\
\frac{d\varphi}{dt} &= \omega_c(z) - e\sqrt{\frac{\omega_c(z)}{2\mu m}}\sum_i \frac{E_{0i}}{\omega_i(z,t)}\sin[\Psi_i(z,t)+\varphi]\ ; \frac{d\mu}{dt} = e\sqrt{\frac{2\mu\omega_c(z)}{m}}\sum_i \frac{E_{0i}}{\omega_i(z,t)}\cos[\Psi_i(z,t)+\varphi]\ ,
\end{aligned} \tag{14}$$

where we have neglected the derivatives with respect to z of slowly varying quantities $\omega_i(z,t), k_i(z,t)$ and E_{0i} in the interaction Hamiltonian.

In the set of equations (14), the quantity φ is an unknown function, while the quantities $\Psi_i(z,t)$ should be considered as known ones. However, the equations of geometrical optics from which the quantities $\Psi_i(z,t)$ should be found define first of all their derivatives, i.e., the quantities $\omega_i(z,t)$ and $k_i(z,t)$. That is why, in the equations of motion (14), it is convenient to use quantities $\zeta_i = \Psi_i(z,t) + \varphi$ as new unknown functions, since the function φ enters the equations of motion only in combinations ζ_i. Thus, instead of equation for φ and equations for $\Psi_i(z,t)$ it is more convenient to use the equations for ζ_i, which follow from the definitions given above and the equation for φ:

$$\frac{d\zeta_i}{dt} = \frac{k_i(z,t)p_\parallel}{m} - \omega_i(z,t) + \omega_c(z) - e\sqrt{\frac{\omega_c(z)}{2\mu m}}\sum_i \frac{E_{0i}}{\omega_i(z,t)}\sin\zeta_i \ . \tag{15}$$

In these equations, the quantities $k_i(z,t)$ and $\omega_i(z,t)$ are the functions that are found directly from the equations of geometrical optics.

The solution of the set of equations (14) for one particle is shown in Figures 10-11. Upper panels of Figure 10 show the variation of latitude and normalized parallel velocity along the particle trajectory. We see that, on large time scale, the particle bounce-oscillates between mirror points occasionally experiencing resonant impacts from the multihop whistler. These impacts change the particle energy and magnetic momentum, the variation taking place during a very short time as compared to bounce period. One of such impacts is zoomed in the bottom right panel of the figure. As one can see from Figures 11, which displays the variation of particle magnetic momentum (upper panel), each impact corresponds to stationary phase point in one of the wave packets, i.e., to the moment at which one of the derivatives $d\zeta_i/dt$ shown in three lower panels turns to zero. We suggest that random jumps of electron energy and magnetic momentum in the course of interaction with multihop whistlers cause particle diffusion in the phase space, which leads to a decrease in free energy of the unstable distribution and the corresponding decrease of the growth rate.

For quantitative estimation of the suggested mechanism, we have calculated the average variation squared, during the duration of the whistler echo train $\Delta t = 2.24\,\mathrm{s}$, of magnetic momentum for 100 particles with initial energy $w = 132\,\mathrm{keV}$ and magnetic momentum such that $\mu\omega_{ceq} = 56.6\,\mathrm{keV}$, uniformly distributed over gyrophases and the accessible range of initial latitudes on $L = 3$. These determine the particle diffusion coefficient $D_{\mu\mu}$

according to the relation

$$D_{\mu\mu} = \frac{\overline{(\Delta\mu)^2}}{2\Delta t} \ .$$

For the parameters of the model described above, the calculations give

$$\frac{\overline{(\Delta\mu)^2}}{\mu^2} = 0.072 \ ,$$

so that $D_{\mu\mu}/\mu^2 \simeq 0.016\,\mathrm{s}^{-1}$. This gives the characteristic diffusion time $t_D \simeq 31\,\mathrm{s}$, which also provides an estimation for the relaxation time of unstable plasma distribution.

4 Concluding remarks

We have presented experimental evidences of VLF noise suppression by strong whistlers which is observed on VLF spectrograms obtained at Kannoslehto ground station, after cleaning them from sferics, as well as on spectrograms obtained on the Van Allen Probe B satellite. The idea that we use to explain this phenomenon can be traced back to early works by *Helliwell et al.* [1980] and *Gail and Carpenter* [1984]. It consists in the assumption that, due to interaction with strong whistler, the unstable electron distribution is modified in such a way that decreases the instability threshold. This modification should first of all be revealed at the boundary of unstable band, as is indeed observed in experiment.

To develop these ideas, we set forth a theory of electron resonant interaction with parallel propagating multihop whistlers. We have derived and solved numerically the set of equations that describe electron motion in the field of three wave packets representing the multihop whistler, and the ambient inhomogeneous geomagnetic field. These equations take into account space-time variations of frequencies and wave vectors in the packets, as well as space-time boundedness of the wave packets. We have shown that resonant interaction with such wave packets leads to electron diffusion in the phase space. We suggest that this diffusion causes the modification of unstable electron distribution and is responsible for the suppression effect.

Acknowledgments

This study was done in the frame of the grant No. 294931 of the Academy of Sciences of Finland. D. R. S. and E. E. T. also acknowledge support from RFBR grant 19-02-00179. O.S. and I.K. acknowledge support from grants LTAUSA17070, GACR 17-07027S, and the Praemium Academiae award from the CAS. The authors thank the PI of EMFISIS instrument C. Kletzing and the PI of MagEIS instrument H. Spence of Van Allen Probes team for the use of the

data which is available at http://cdaweb.sci.gsfc.nasa.gov/istp_public/. SGO ELF-VLF quick-look plots are available at http://www.sgo.fi/pub_vlf/.

References

Blake, J. B. et al. (2013), The Magnetic Electron Ion Spectrometer (MagEIS) Instruments Aboard the Radiation Belt Storm Probes (RBSP) Spacecraft, *Space Science Reviews*, doi: 10.1007/s11214-013-9991-8.

C. A. Kletzing, W. S. Kurth, M. Acuna, R. J. MacDowall, R. B. Torbert, T. Averkamp, D. Bodet, S. R. Bounds, M. Chutter, J. Connerney, D. Crawford, J. Dolan, R. Dvorsky, G. Hospodarsky, J. Howard, V. Jordanova, R. Johnson, D. Kirchner, B. Mokrzycki, G. Needel, J. Odom, D. Mark, J. Phillips, C. Piker, S. Remington, O. Santolik, R. Schnurr, D. Sheppard, C. W. Smith, R. M. Thorne, & J. Tyler (2013), The Electric and Magnetic Field Instrument Suite and Integrated Science (EMFISIS) on RBSP, *Space Sci. Rev.*, *179*, 127–181, doi: 10.1007/s11214-013-9993-6.

Cornilleau-Wehrlin, N, J. Solomon, A. Korth, & G. Kremser (1985), Experimental study of the relationship between energetic electrons and ELF waves observed on board GEOS: a support to quasi-linear theory, *J. Geophys. Res*, *90*, 4141–4154.

Gail, W. B., & D. L. Carpenter (1984), Whistler induced suppression of VLF noise, *J. Geophys. Res.*, *89*(2), 1015–1022.

Helliwell, R. A., S. B. Mende, J. H. Doolittle, W. C. Armstrong, & D. L. Carpenter (1980), Correlations between λ4278 optical emissions and VLF wave events observed at $L \sim 4$ in the Antarctic, *J. Geophys. Res.*, *85*, 3376-3386.

Inan, U. S., & T. F. Bell (1977), The plasmapause as a VLF wave guide, *J. Geophys. Res.*, *82(19)*, 2819-2827, doi:10.1029/JA082i019p02819.

Jyrki Manninen, Tauno Turunen, Natalia Kleimenova, Michael Rycroft, Liudmila Gromova, & Iina Sirviö (2016), Unusually high frequency natural VLF radio emissions observed during daytime in Northern Finland, *Environ. Res. Lett.*, *11*, 124006, doi:10.1088/1748-9326/11/12/124006.

Kurth, W. S., S. De Pascuale, J. B. Faden, C. A. Kletzing, G. B. Hospodarsky, S. Thaller, & J. R. Wygant (2015), Electron densities inferred from plasma wave spectra obtained by the waves instrument on Van Allen Probes, *Journal of Geophysical Research: Space Physics*, *120*, 904–914, https://doi.org/10.1002/2014JA020857.

Ostapenko, A. A., E. E. Titova, A. P. Nickolaenko, T. Turunen, J. Manninen, & T. Raita (2010), Characteristics of VLF atmospherics near the resonance frequency of the Earth-ionosphere waveguide 1.62.3 kHz by observations in the auroral region, *Ann. Geophys.*, *28*, 193-202.

Platino, M., U. S. Inan, T. F. Bell, D. A. Gurnett, J. S. Pickett, P. Canu, & P. M. E. Décréau (2005), Whistlers observed by the Cluster spacecraft outside the plasmasphere, *J. Geophys. Res.*, *110*, A03212, doi:10.1029/2004JA010730.

Sagdeev, R. Z. and V. D. Shafranov (1961), On the instability of a plasma with an anisotropic distribution of velocities in a magnetic field, *Sov. Phys. JETP*, *12*, 130–132.

Santolk, O., J. S. Pickett, D. A. Gurnett, & L.R.O. Storey (2002), Magnetic component of narrow-band ion cyclotron waves in the auroral zone, *J. Geophys. Res.*, *107*(A12), 1444. https://doi.org/10.1029/2001JA000146.

Santolk, O., Parrot, M., & Lefeuvre, F. (2003). Singular value decomposition methods for wave propagation analysis, *Radio Science*, *38*(1), 1010. https://doi.org/10.1029/2000RS002523.

Santolk, O., J. S. Pickett, D. A. Gurnett, J. D. Menietti, B. T. Tsurutani, & O. Verkhoglyadova (2010), Survey of Poynting flux of whistler mode chorus in the outer zone, *J. Geophys. Res.*, *115*, A00F13. doi:10.1029/2009JA014925.

Semenova, V. I., & V. Yu. Trakhtengerts (1980), On specific features of the LF waveguide propagation, *Geomagn. Aeron*, *20*(6), 1021-1027.

Shklyar, D., & H. Matsumoto (2009), Oblique whistler-mode waves in the inhomogeneous magnetospheric plasma: Resonant interactions with energetic charged particles, *Surveys in geophysics*, *30*(2), 55–104.

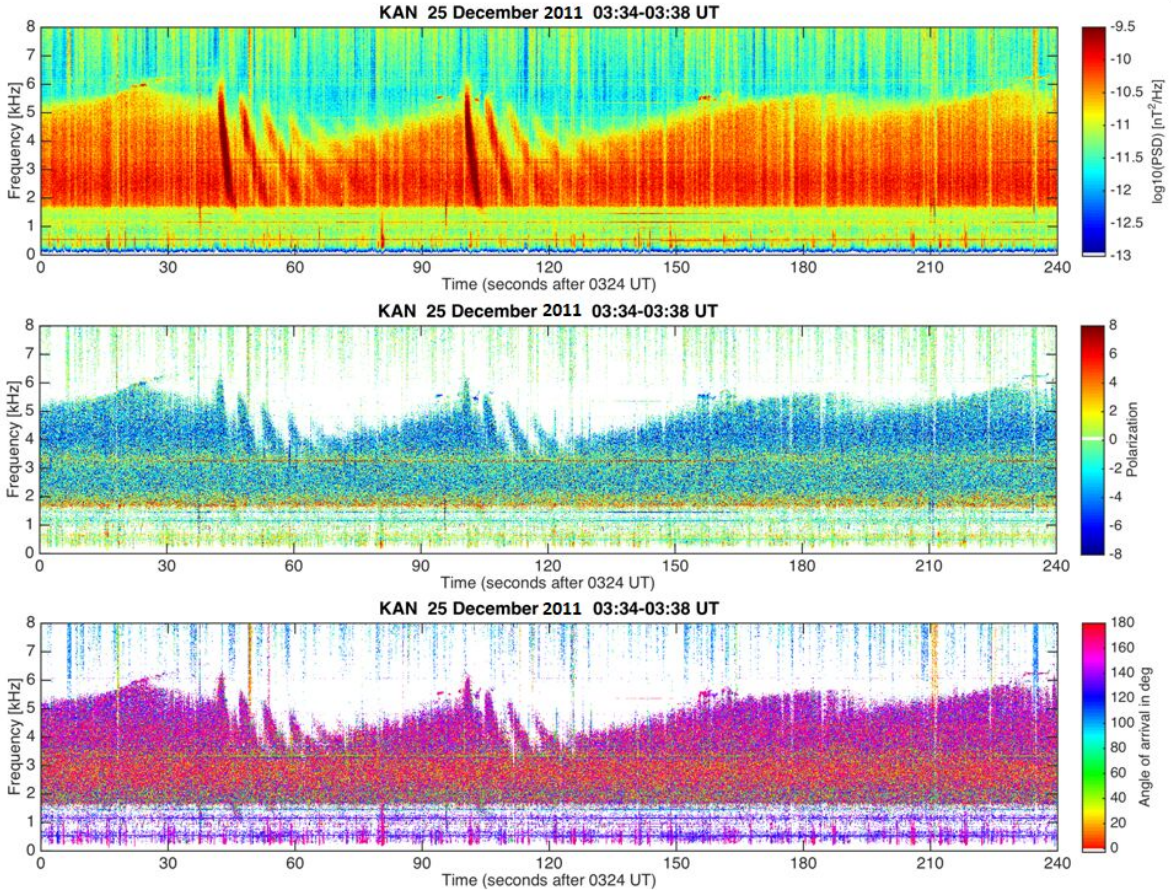

346 **Figure 1.** An example of spectrogram, obtained from ground station data, illustrating whistler induced
347 suppression of VLF noise. (a) Logarithm of the total magnetic field power spectral density. (b) Parameter
348 characterizing the wave polarization (see the text). (c) The angle between minor axis of the wave polarization
349 ellipse and the north-south direction.

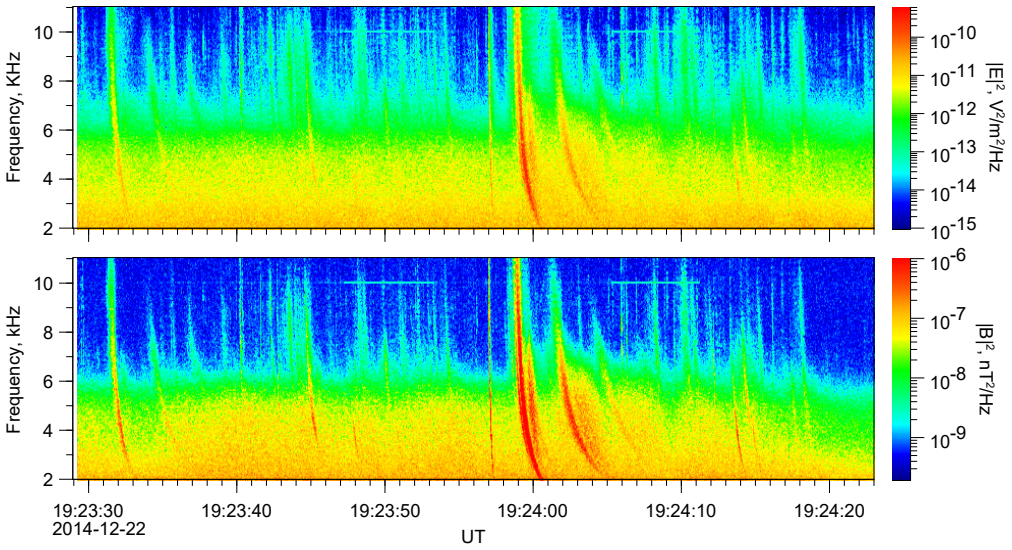

Figure 2. Dynamic spectra of VLF emission computed from RBSP-B waveform data for wave event observed on 22 December 2014. The sum of the power spectral densities of three orthogonal (a) electric and (b) magnetic components.

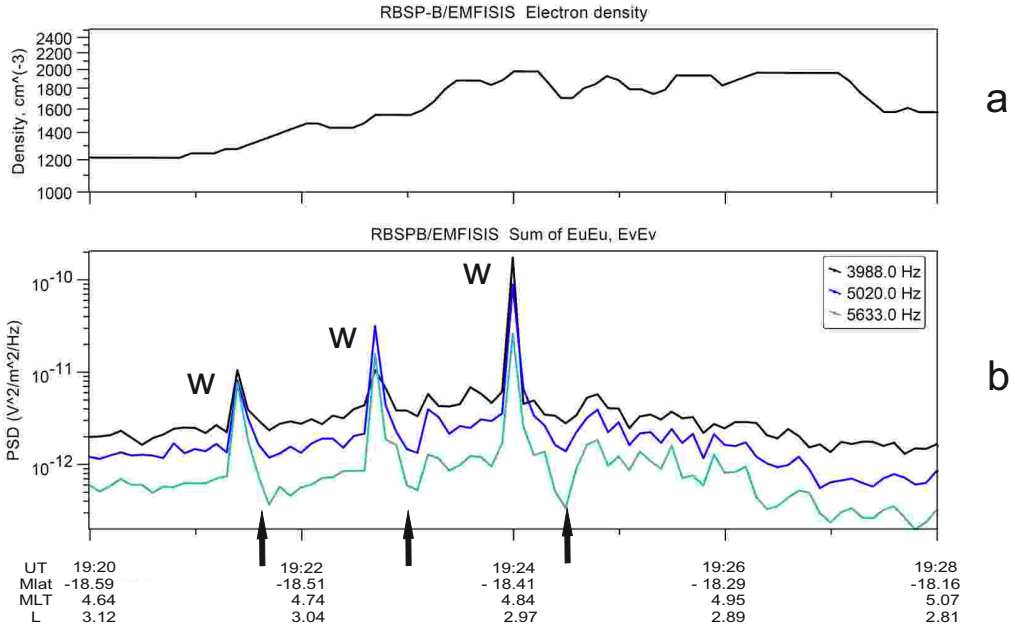

Figure 3. (a) Cold plasma density measured by RBSP-B. (b) Electric field spectral power of VLF emission detected in three frequency channels centered on 3988, 5020, and 5633 Hz.

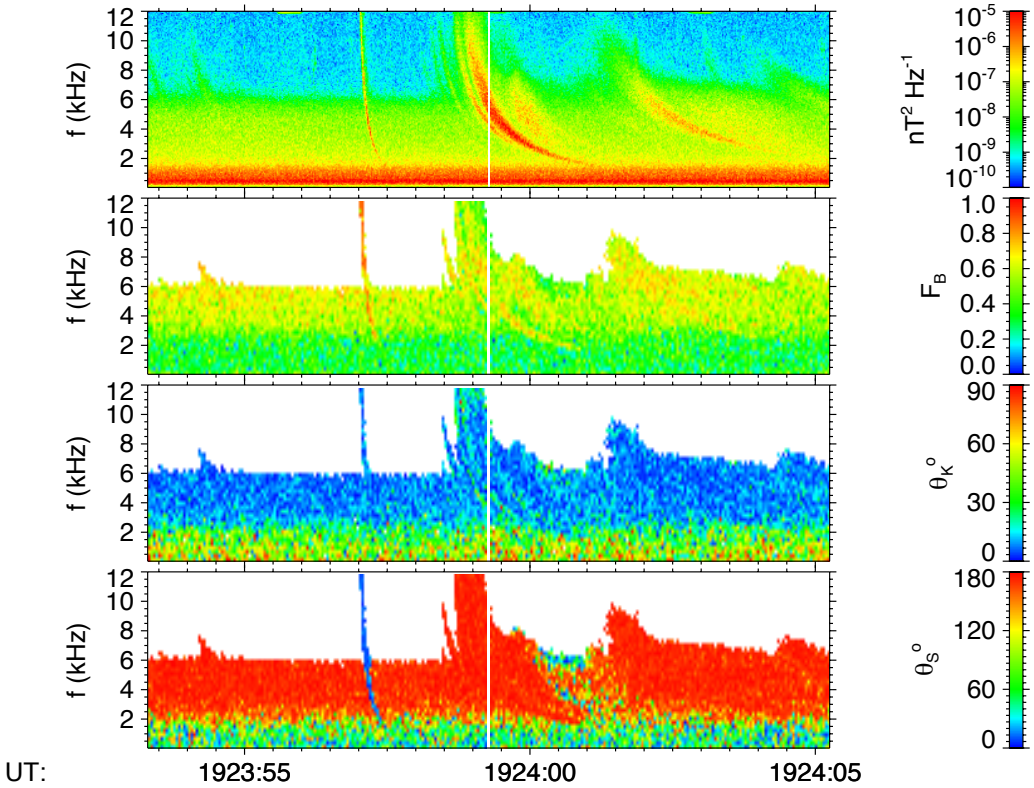

Figure 4. The results of multicomponent analysis of VLF wave measurements by RBSP-B on 22 December 2014 (see text for explanation of the displayed quantities).

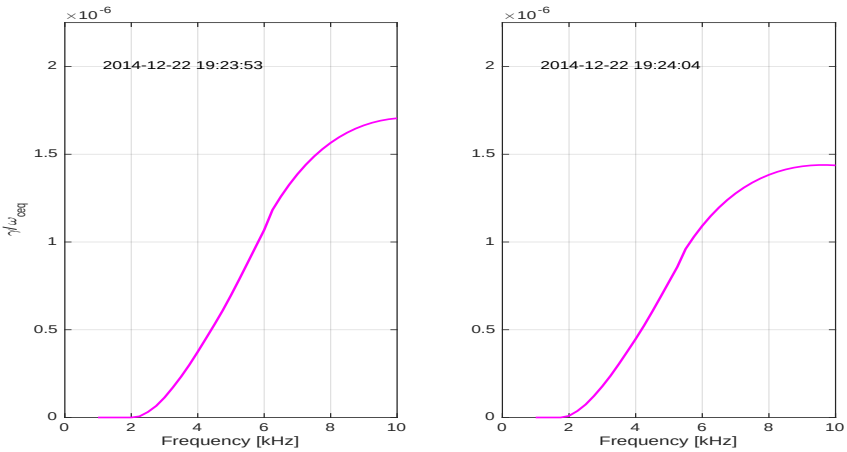

Figure 5. Growth rate as a function of frequency for parallel propagating whistler-mode waves calculated from RBSP-B measurements of electron fluxes by MagEIS instrument. Left and right panels display the normalized growth rate before and after the third whistler shown in Figure 3.

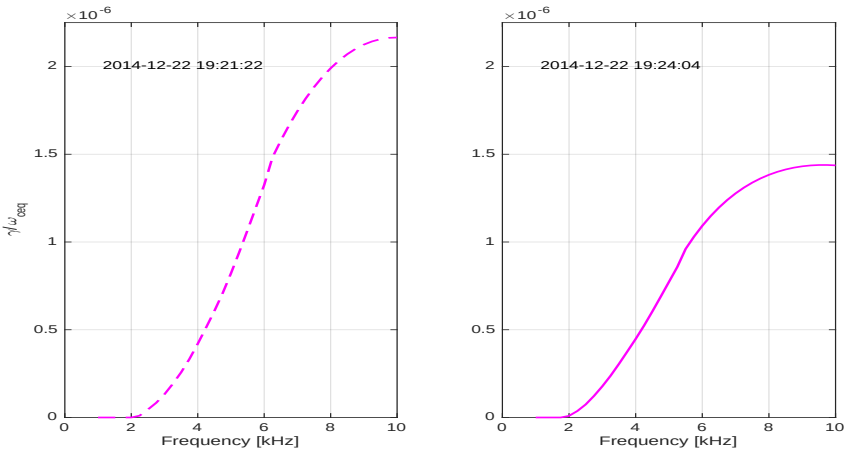

Figure 6. Just like above, but for moments before and after the series of whistlers shown in Figure 3.

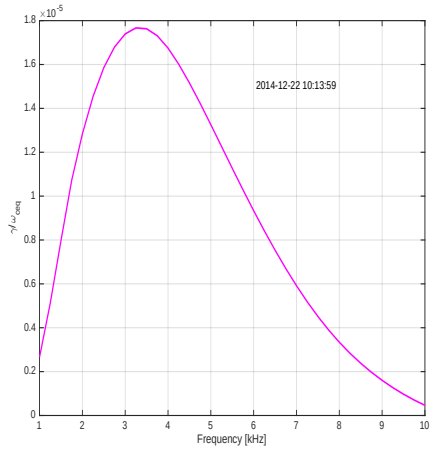

Figure 7. Growth rate at the equator ($L = 3.09, \ \lambda = 0.75^o$) as a function of frequency calculated from electron fluxes measured by MagEIS instrument on RBSP-B on 22 December 2012, at 10:13:59 UT.

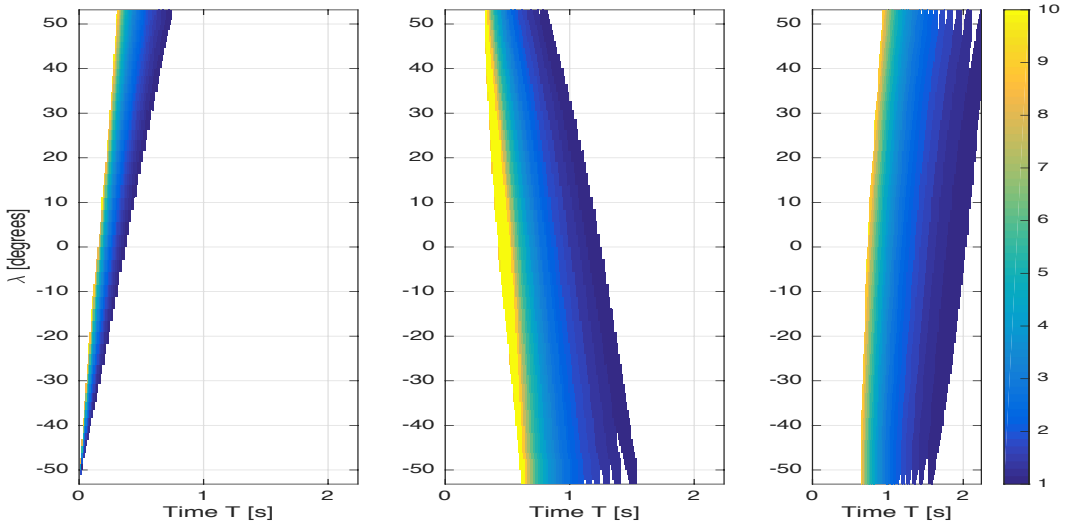

Figure 8. Frequency in kHz, colorcoded according to the colorbar, in space-time domain of three wave packets corresponding to multihop whistler: (left) fractional-hop whistler, (middle) second-hop whistler reflected from the ground in the northern hemisphere, and (right) third-hop whistler reflected from the ground in the southern hemisphere.

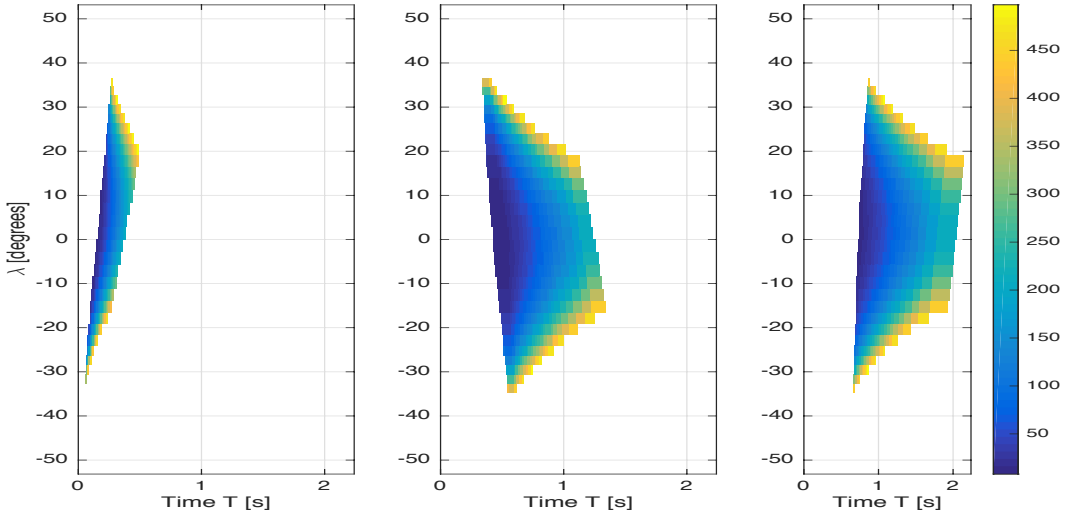

Figure 9. Resonance energy in keV, colorcoded according to colorbar, in space-time domain for three wave packets corresponding to multihop whistler (see the caption to Figure 8). Only domains where the resonance energy calculated according to non-relativistic expression is below 500 keV are displayed.

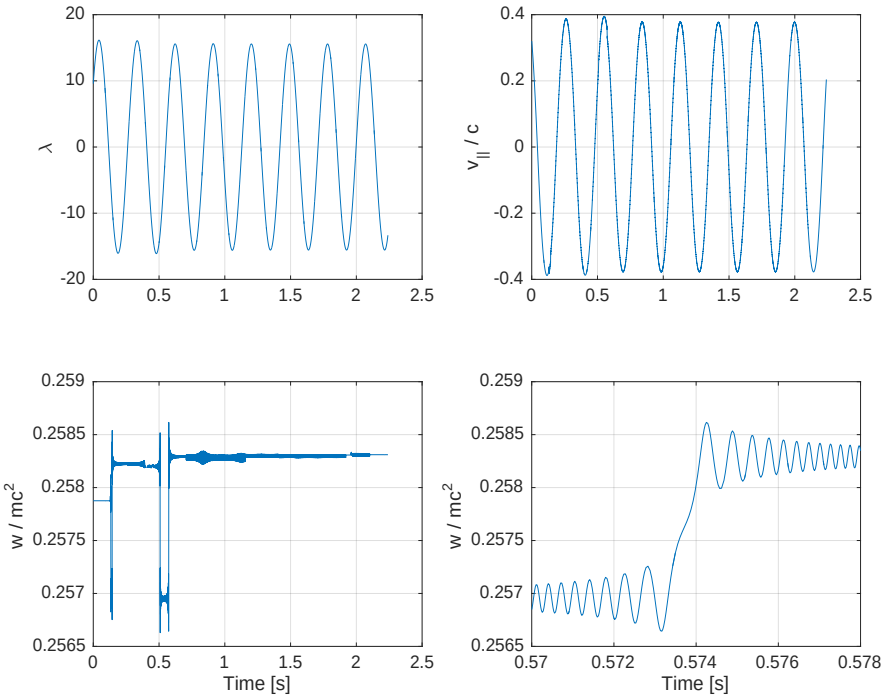

Figure 10. Time variations of particle latitude λ, longitudinal velocity $v_{\|}$, and kinetic energy w along the trajectory in the field of multihip whistler and the ambient geomagnetic field. Initial parameters of the particle are as follows: $\lambda_0 = 9.5865^o$; $v_{\|0} = 0.32\,\mathrm{c}$; $\zeta_{1,0} = 6.0287\,\mathrm{rad}$; $\mu_0\omega_{ceq} = 0.1825\,\mathrm{mc}^2$; $w_0 = 0.2579\,\mathrm{mc}^2$. The particle moves along $L = 3$ where electron cyclotron frequency at the equator $\omega_{ceq} = 2.02 \cdot 10^5$ rad.

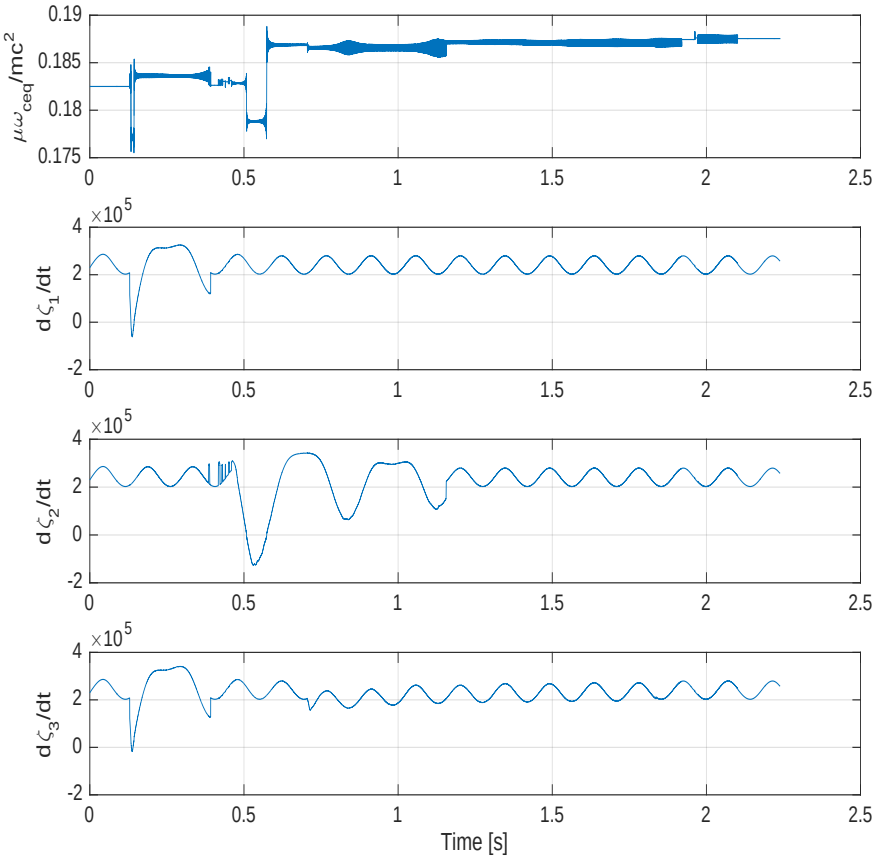

374 **Figure 11.** Time variations of particle magnetic momentum and derivatives of the phases of three wave
375 packets representing multihop whistler. Initial conditions are the same as in the Figure 10.